Supplementary Information (SI) for Nanoscale.
This journal is © The Royal Society of Chemistry 2024

Supplementary Information for

Laser-assisted Thermoelectric-enhanced Hydrogen Peroxide Biosensor Based on Ag_2Se Nanofilms for Sensitive Detection of Bacterial Pathogens

Huangshui Ma [a, g,#], *Shiyu Pu* [b,#], *Shiyu Jia* [a], *Shengduo Xu*[c], *Qiwei Yu* [d], *Lei Yang* [e,*], *Hao Wu* [f,*], *Qiang Sun* [a, g,*]

[a] State Key Laboratory of Oral Diseases, National Center for Stomatology, National Clinical Research Center for Oral Diseases, West China Hospital of Stomatology, Sichuan University, Chengdu 610041, China

[b] Department of Ultrasonography, West China Second University Hospital, Sichuan University, Chengdu 610041, China

[c] Institute of Science and Technology Austria (ISTA), Klosterneuburg 3400, Austria

[d] The First Clinical College, Changsha Medical University, Changsha 410005, China.

[e] College of Materials Science and Engineering, Sichuan University, Chengdu 610065 China

[f] Department of Stomatology, The First Medical Centre, Chinese PLA General Hospital, Beijing 100039, China

[g] Sichuan Provincial Engineering Research Center of Oral Biomaterials, Chengdu 610064, China

*Corresponding author: E-mail: *lyang1986@scu.edu.cn*, *wh_dds@126.com* *qiangsun@scu.edu.cn*

Section 1. Experimental Details

1.1. Materials Synthesis:

H_2O_2, alcohol, glycine, glycerol, NaCl, Urea, horseradish peroxidase (HRP), 2,2′-azino-bis(3-ethylbenzothiazoline-6-sulfonicacid) (ABTS), Se powder (99.99%) was purchased from Shanghai Aladdin Bio-Chem Technology Co. Ltd. China. $Na_2S·9H_2O$ (98.0%) was purchased from Shanghai Aladdin Bio-Chem Technology Co. Ltd. China. The H_2O_2 test assay kit and ROS stain kit were purchased from Beyotime Biotechnology (Shanghai, China). All chemicals were used without further purification. Deionized water was purified using a Milli-Q Direct 8 ultrapure water system (MilliporeSigma).

1.2. Preparation of Ag_2Se Films on 3D-printing Resin Substrates:

The Ag film precursors were fabricated on the PE substrate using a magnetron sputtering instrument (GU-SP2000, Guangzhou L-Victror Tycoon Co. Ltd., China). Prior to sputtering, commercial PE substrates of various thicknesses were cleaned by ultrasonic treatment in isopropanol for 30 min, followed by drying in a drying oven for subsequent use. The cleaned PE substrates were affixed to the sample stage of the sputtering apparatus with tape. The distance between the Ag target and the PE substrate was maintained at approximately 50 mm. In this sputtering setup, the operating current values were automatically regulated by the sputtering system. The Ag deposition onto the clean PE substrates was conducted in an Ar_2 atmosphere after the chamber vacuum was pumped to $1×10^{-2}$ mbar; during the sputtering process, the vacuum was maintained at $4×10^{-2}$ mbar. With an operating current of 20 mA, the thickness of the Ag films was precisely controlled by the sputtering duration, as verified by a film thickness tester. The Se precursor solution was prepared following a previously reported method: 0.6 g of $Na_2S·9H_2O$ (98.0%) was dissolved in 20 ml of deionized water, followed by the dissolution of 0.2 g of Se powder (99.99%) in the Na2S aqueous solution. After stirring, the solution's color transitioned from colorless to dark red, signifying the formation of the Se precursor aqueous solution. To produce Ag_2Se films, the Ag-coated PE substrates were immersed in the Se/Na_2S solution for roughly 30 s at

room temperature. The complete conversion to Ag_2Se films was indicated by a color change from silver to grey. Subsequently, the Ag_2Se films were rinsed with deionized water and allowed to dry naturally at room temperature. The entire process was conducted at room temperature (25 ℃) in an ambient air environment.

1.3. Structural and Compositional Characterization:

The morphology of obtained Ag and Ag_2Se films were examined with scanning electron microscopy (SEM) (FEI ESCALAB Xi+), with an operating voltage of 10 KeV. The cross-sectional TEM specimen was prepared by a FIB (Focused Ion Beam) system, Thermo Scientific Helios 5 CX. TEM characterization was performed by Talos F200S, Thermo Fisher (at the accelerating voltage of 200 kV), equipped with SuperX EDS detector for compositional analysis. X-ray photoelectron spectroscopy (XPS) was performed using FEI ESCALAB Xi+. Grazing Incidence X-ray Diffraction (GIXRD) w as performed on the Ag_2Se thin layer with different thicknesses to examine the phase using Smartlab 9KW.

1.4. Thermoelectric Properties Measurement:

The temperature-dependent Seebeck coefficient (S) and electrical conductivity (σ) of obtained Ag_2Se films were measured by a lab-made instrument in the temperature from 298K to 363K, during which the morphology of PE substrates can be well maintained. Power factors of obtained films were obtained according to $PF = S^2\sigma$. The electrical voltage behavior of Ag_2Se films of various thicknesses was evaluated upon exposure to a steady heat flux, and the data were meticulously recorded using a DMM6500 Keithley digital multimeter.

1.5. Substrate Recognition Specificity and Device Performance of the Ag_2Se-based Biosensor:

To illustrate the specificity of the Ag_2Se-based biosensor, a series of substances including alcohol, glycine, glycerol, NaCl, urea, and H_2O_2 (each at a final concentration of 4 μM) were individually introduced into the standard solution containing HRP and ABTS, which was then incubated for 30 seconds. Following this incubation, 500 μl the solution was added to the biosensor and subjected to 808 nm laser irradiation for 60

seconds, after which the voltage signals generated by the temperature difference were recorded. To demonstrate the sensitivity of the Ag_2Se-based biosensor, various concentrations (from 0-10 μM) of H_2O_2 were individually introduced into a solution containing HRP and ABTS, which was then incubated for 5 minutes. Following this incubation, the solution was tested by the biosensor in the same way. After the incubation period, the solution was analyzed consistently using the biosensor. The voltage signals were recorded by a digital multimeter (DMM6500 Keithley).

1.6. Detection of Hydrogen Peroxide in Beverage:

Milk, soda water, and lemonade were sourced from a local market. These beverage samples were spiked with H_2O_2 at concentrations from 0 to 10 μM. A measured amount of chloroacetic acid was added to facilitate protein precipitation in the milk. The milk was then sonicated for 20 minutes and centrifuged at 5,000 rpm for a 5-minute duration to isolate the protein precipitate. Subsequently, the supernatants from the milk treatment, alongside the H_2O_2-spiked soda water and lemonade samples, were each combined with a standard solution in equal parts. These prepared samples were then evaluated using the Ag_2Se-based biosensor for analysis.

1.7. Hydrogen Peroxide Detection Using Assay Kit:

The solution sample is incubated with the detection reagents provided in the kit for half an hour, after which the absorbance is measured using a microplate reader. Subsequently, the H_2O_2 concentration is calculated using the standard curve.

1.8. Reactive Oxygen Species Detection Using Assay Kit:

Adjust the concentration of DCFH-DA to a final concentration of 10 μM. Subsequently, mix the bacteria with DCFH-DA and incubate at 37°C for 20 minutes. After the incubation time, centrifuge the mixture at 5000 rpm for 5 minutes to separate the bacteria. Then, gently resuspend the bacteria in PBS and perform a three-wash step to wash the bacteria. After the washing process is complete, observe the bacteria using a fluorescence microscope.

1.9. Bacterial Culture：

A single *Methicillin-resistant Staphylococcus aureus* (MRSA) strain colony was inoculated and grown in 5 mL of Luria−Bertani (LB) media overnight under aerobic

conditions. *S. sanguinis* was cultured overnight in a Brain Heart Infusion (BHI) medium under anaerobic conditions.

1.10. SEM investigation of Bacterial:

The obtained bacteria were fixed with a primary fixative such as 2.5% glutaraldehyde in a buffer solution for 1 hour. After fixing, a series of dehydration steps were performed using increasing concentrations of ethanol (e.g., 30%, 50%, 70%, 90%, and 100%) to replace the water within the cells with ethanol.

1.11 *S. sanguinis* Detection with Different Concentration：

Various concentrations (2 to 10 × 10^5 CFU/ml) of *S. sanguinis* were cultivated in the BHI medium within an anaerobic environment for one hour. After the incubation, the bacterial cultures underwent centrifugation at 5000 rpm for 5 minutes to isolate the supernatant. The supernatant was next blended with the standard solution and underwent a further 5-minute incubation. Following this, it was subjected to analysis by an Ag_2Se-based sensor, and the resultant voltage measurements were recorded using the DM6500 instrument.

1.12 *MRSA* Detection with Different Concentrations:

Various concentrations of *MRSA* (2 to 10 × 10^5 CFU/ml) were subjected to a 5-minute incubation with a corresponding concentration of H_2O_2. After this incubation, the mixture was centrifuged for 5 minutes to isolate the supernatant. This supernatant was then mixed with the standard solution in the same volume incubated for an additional 5 minutes, and then examined by the Ag_2Se-based biosensor.

Section 2 Additional Characterization of Ag_2Se films

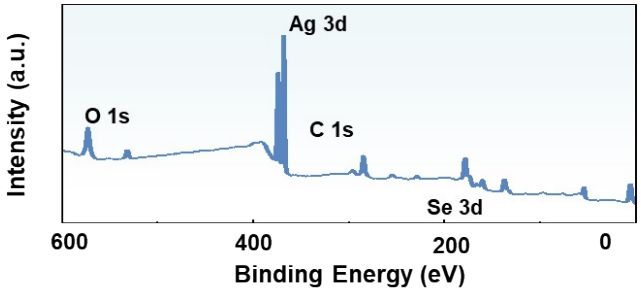

Fig. S1. X-ray photoelectron spectroscopy spectrum of Ag_2Se film.

Fig. S1 shows the full X-ray photoelectron spectroscopy (XPS) spectrum of Ag_2Se, which examines the chemical characteristics of the obtained Ag_2Se film, including the characteristic peaks of Ag $3d_{3/2}$, Ag $3d_{5/2}$, Se $3d_{3/2}$, and Se $3d_{5/2}$, existing in Ag2Se compounds. The full XPS spectrum reveals that pure Ag_2Se was synthesized successfully.

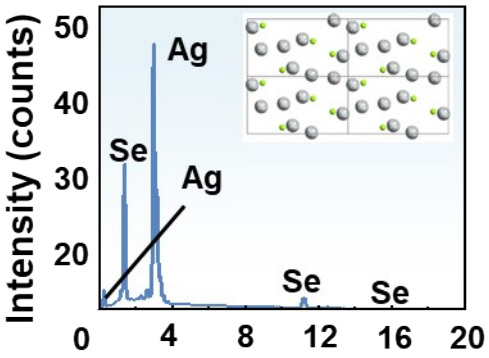

Fig. S2 Energy dispersive spectrum (EDS) showing the composition of Ag_2Se.

Fig. S2 shows that EDS point analysis was carried out to corroborate the compositional concentrations of the synthesized Ag_2Se films, and the results align with the theoretical stoichiometric ratio of Ag_2Se.

Section S3. Properties of Ag_2Se film

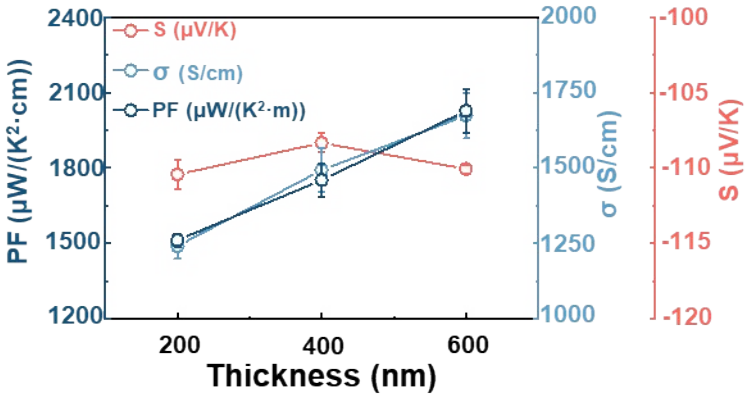

Fig. S3. Seebeck coefficient *S*, electrical conductivity σ, and power factor *(PF)* of Ag_2Se film with various thicknesses at room temperature.

Fig. S3. shows that Ag_2Se nanofilms deposited on a resin substrate displayed a relatively stable Seebeck coefficient regardless of the thickness, which is expected to ensure the stability of sensor performance. While the thickness of the Ag_2Se nanofilms increases, the σ of the films also increases, thereby leading to an increase in the *PF*.

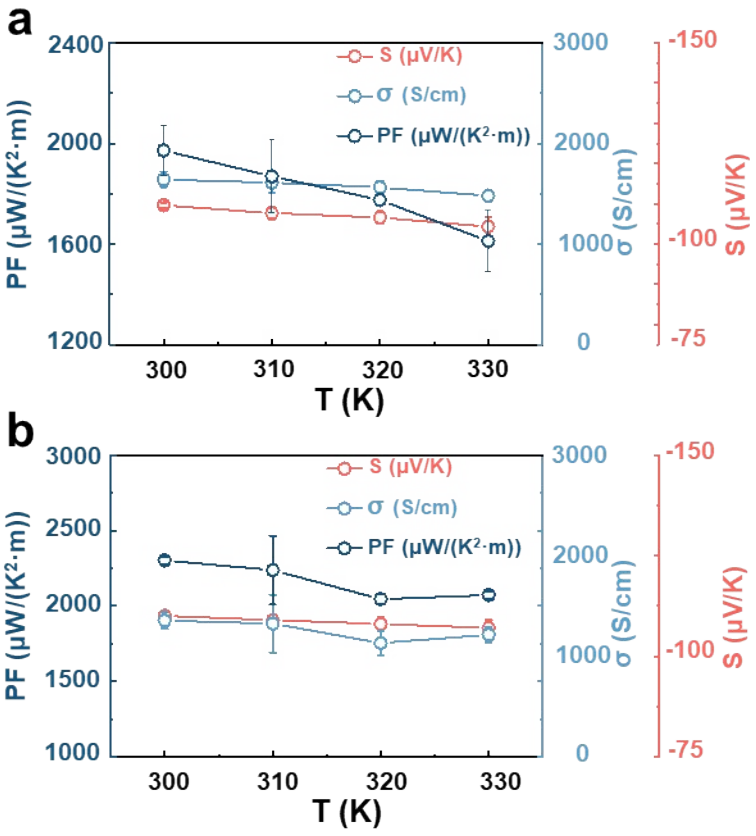

Fig. S4. Temperature-dependent thermoelectric (TE) performance of Ag_2Se films with thicknesses of 400 nm (a) and 600 nm (b).

Fig. S4 provides the detailed TE performance of Ag_2Se films with different thicknesses near room temperatures. With the elevation of temperature, the *S* for Ag_2Se films of disparate thicknesses exhibits a modest downturn, all the while sustaining values above 100 μV/K within the 295-330 K temperature spectrum, consistent with the thermoelectric properties of β-Ag_2Se. Concurrently, the electrical conductivity maintains a relatively stable level at approximately 1500 S/cm. Following the power factor (*PF*) computation, the *PF* of Ag_2Se films, irrespective of thickness, diminishes as the temperature ascends.

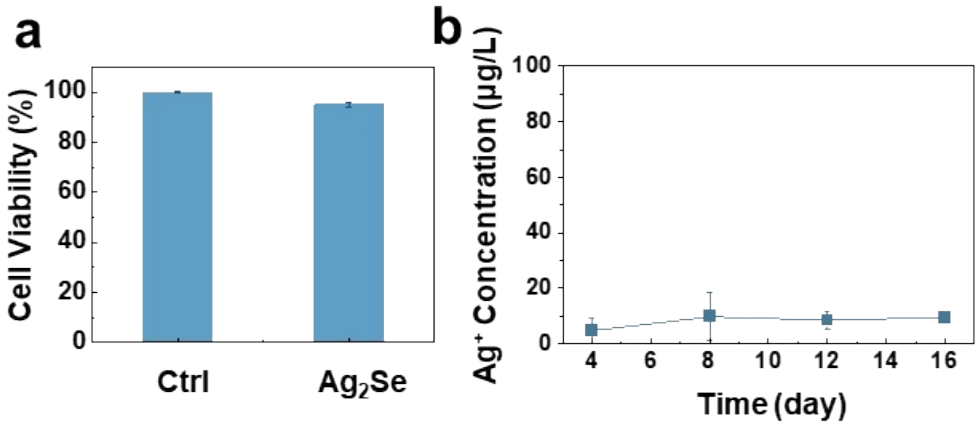

Fig. S5. (a) Assessment of HUVEC activity after Co-Incubation with Ag_2Se films. (b) The release of Ag ions from Ag_2Se films was measured over various time periods ranging from 4 to 16 days.

Section S4. Fabrication and Performance of the Ag_2Se-based TE biosensors

This section provides additional information on the fabrication process and performance of the Ag_2Se-based TE biosensor. **Fig. S6** shows the schematic illustration of the TE biosensor, and **Fig. S7** displays the photo of the biosensor assembled. To evaluate the H_2O_2 detection capabilities of our biosensors, its detection limit was compared to other techniques.

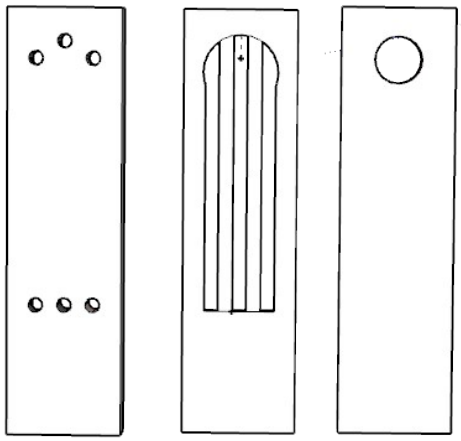

Fig. S6. Design of a 3D model for the Ag_2Se-based TE biosensor.

The models used in the 3D printing are shown in **Fig. S6**. The model on the left represents the sensor substrate, the central model corresponds to the masking layer, and the model on the right constitutes the sensor's protective encapsulation.

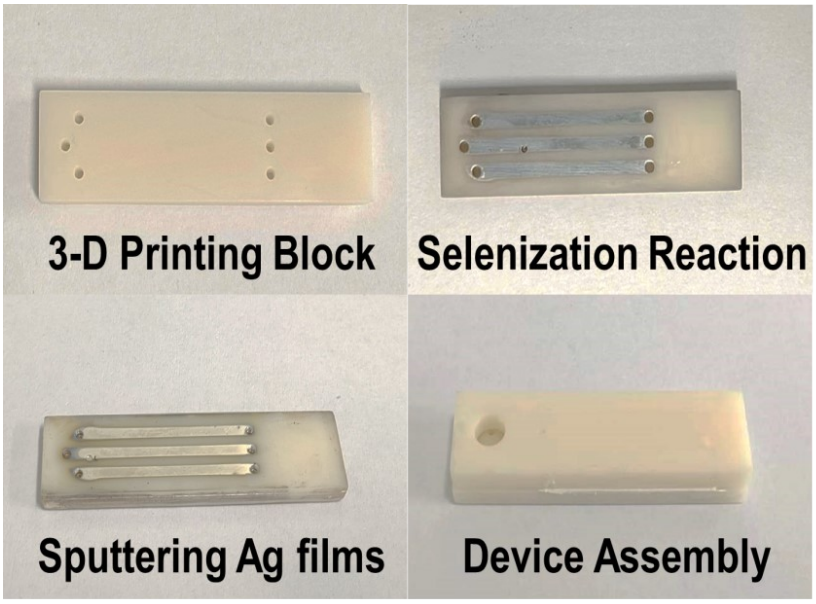

Fig. S7. Photograph of the assembled Ag_2Se-based TE biosensor, depicting the process of constructing the biosensor.

Fig. S7 shows the process of building the Ag_2Se-based TE biosensor. First, the 3D resin block was printed by the printer, and after masking with **Fig S6**, a silver film was sputtered. Subsequently, the film was treated with a Na_2S/Se solution for selenization to synthesize Ag_2Se films. Then, the circuit was connected using Ag_2Se, and after PI encapsulation, a 3D-printed protective layer was applied.

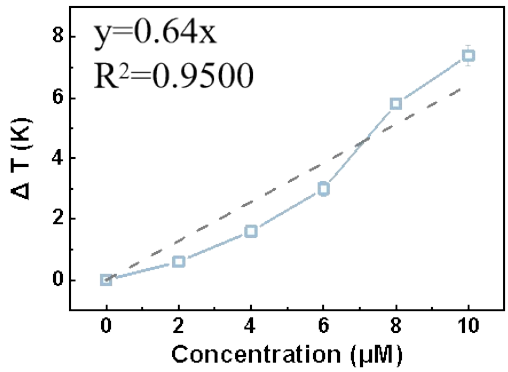

Fig. S8 The heat release difference under laser was observed for the test solution incubated with various concentrations of H_2O_2, and the results were analyzed theoretically with the sensor's response.

The chemical equation for the catalytic oxidation of ABTS into ABTS radicals by H_2O_2,

facilitated by HRP, indicates that a 1M concentration of ABTS will produce a corresponding 1M concentration of ABTS radicals ($ABTS^{\cdot+}$).

$$ABTS + H_2O \xrightarrow{HRP} ABTS^{\cdot+} + 2H_2O$$

These radicals are capable of generating increased heat when exposed to an 808 nm laser. However, the precise quantification of this heat is complicated by various factors, including laser-to-sample distance, container volume, the specific heat capacity of the container, and the volume of the liquid, all of which influence the temperature change induced by the heat produced from $ABTS^{\cdot+}$. As a result, deriving a theoretical formula is challenging. Consequently, we conducted experiments to measure the temperature increment resulting from the $ABTS^{\cdot+}$ at varying concentrations of H_2O_2 in the presence of HRP, as compared to non-oxidized ABTS (Fig. S8). This allowed us to establish a correlation between temperature and H_2O_2 concentration. Due to the insulating effect of the PI film, only a fraction of the generated heat is transferred to the Ag_2Se, which is then further amplified by the three-legged device. The voltage generated by the Ag_2Se thermoelectric sensor in response to the oxidation of ABTS by H_2O_2 is therefore equal to the temperature rise in the solution due to the heat released from the reaction, multiplied by the thermal impedance factor of the PI film, the amplification factor of the three-legged thermoelectric device. Therefore, the relationship between the voltage and the H_2O_2 concentration is as follows:

$$\Delta V = c \times \Delta T \times \alpha \times \beta \times S$$

c refers to the concentration of H_2O_2, ΔT represents the greater temperature rise of the liquid containing $ABTS^{\cdot+}$ compared to non-oxidized ABTS when exposed to the 808 nm laser, α is the proportion of temperature conducted to the Ag_2Se due to the barrier of the PI film, β is the amplification factor of the three-legged device, S is the Seebeck coefficient of Ag_2Se (-110 μV/K). Therefore, we can obtain the following formula:

$$c = \Delta V / 70.4\, \alpha\, \beta$$

The fitting curve of the test results is $= \Delta V / 77.6$ (Fig. 3f), indicating that the product of α and β is greater than 1, which means that the design of the three-legged device compensates for the negative thermal insulation effect brought by PI, and is beneficial

to improve the accuracy of the sensor.

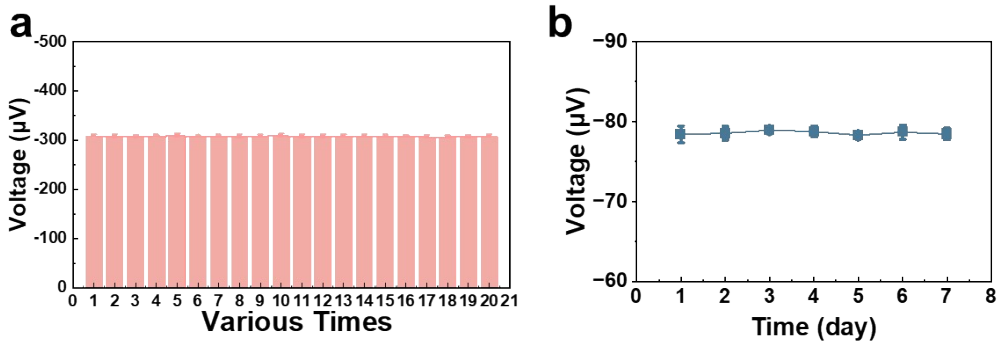

Fig S9 Repeatability and Stability Assessment of the Sensor (a) Repeatability of sensor measurements under consistent H_2O_2 concentration. (b) Stability of sensor performance over a seven-day period.

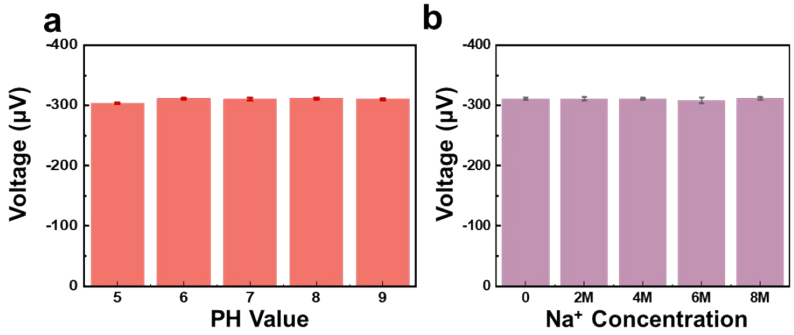

Fig S10 The voltage response of the sensor under different pH levels (a) and Na^+ concentrations (b).

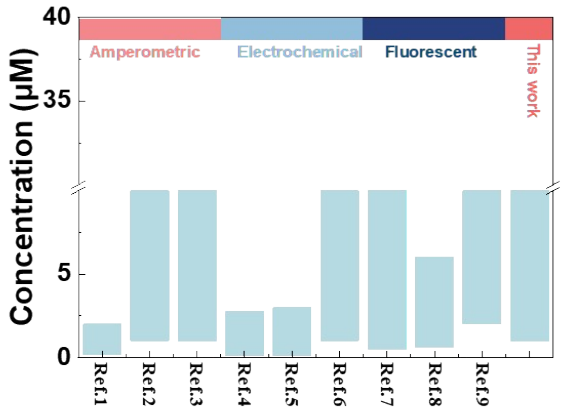

Fig. S11. The H_2O_2 detection capabilities were compared to the findings presented in this work and reported studies [1-9].

Fig. S7 illustrates that by comparing our sensor with the recently developed H_2O_2 sensors that utilize amperometry, electrochemical, or fluorescent detection techniques, it is evident that our sensor exhibits comparable performance. However, it stands out with a notable advantage: it possesses a significantly lower detection limit. This feature makes our sensor more sensitive and capable of detecting lower concentrations of hydrogen peroxide, which is critical for applications requiring high precision and sensitivity in analytical measurements.

Section S5. Morphology of *S. sanguinis* tested by the Ag_2Se-based TE biosensor.

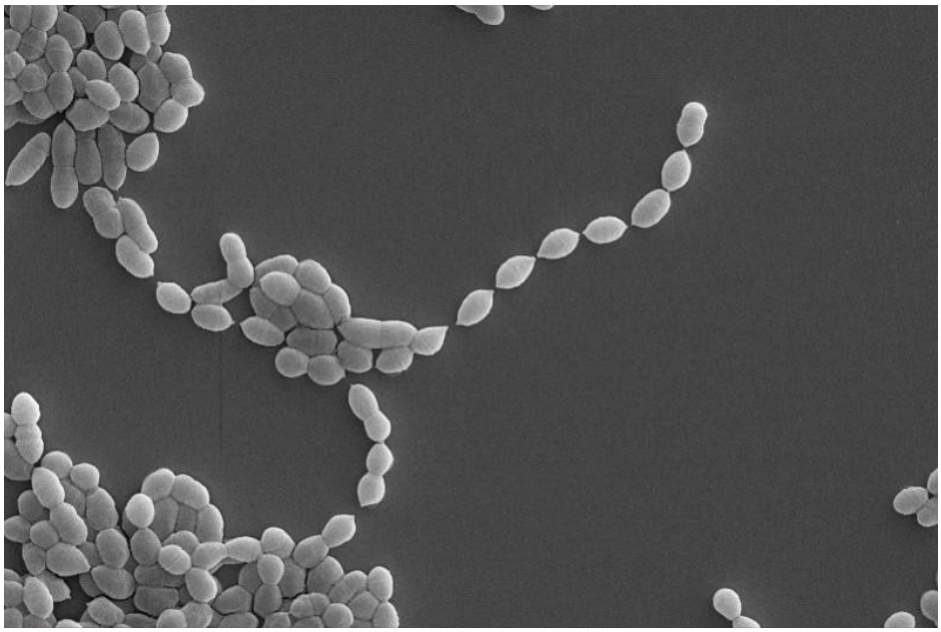

Fig. S12. SEM image of *S. sanguinis*, depicting the characteristic chain-like structure of the bacterium.

Fig. S12 shows the SEM image of *S. sanguinis*, illustrating the typical microbial morphology. The bacteria are arranged in a linear chain pattern, with each cell neatly aligned next to the other, displaying a smooth and uniform morphology without any surface irregularities or folds.

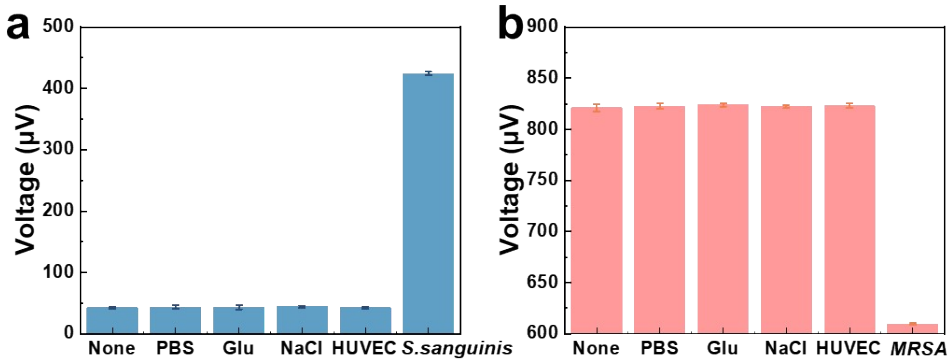

Fig. S13. Specificity analysis of the sensor for *S. sanguinis* and *MRSA*.

Table S1 Comparison of the performance of H_2O_2 biosensors against the Ag_2Se-based biosensor.

Response time (s)	Stability[days]	Mechanism	Sensitivity	Operation	Equipment requirements	Ref
5	10	Amperometric	Medium	Medium	Medium	10
3600	7	Chemiresistive	High	Medium	Medium	11
3600	-	Colorimetric	High	Simple	Medium	12
3600	-	Fluorescent	Low	Medium	Simple	13
600	-	Amperometric	Medium	Complex	Sophisticated	14
3600	-	Potentiometric	High	Complex	Sophisticated	15
3	14	Amperometric	High	Complex	Medium	16
4	60 min	Amperometric	High	High	Sophisticated	17
300	20	Thermoelectric	Medium	Simple	Simple	This work

Table S2 Comparison of biosensor performance with different thermoelectric materials versus the Ag_2Se-based biosensor.

Material	Response Time	Bacterial Detection	Biocompatibility	Reusable	Ref
PEDOT: PSS	10 min	No	-	Yes	18
In_2S_3	＞13 min	No	No	No	19
Sb/Bi	＞3 min	No	No	Yes	20
Bi_2Te_3	＞3 h	No	Yes	No	21
Bi_2Te_3	＞3 h	No	-	Yes	22
Bi_2Te_3	-	No	No	Yes	23
Bi NWs	100 min	No	No	No	24
SnSe	-	No	Yes	No	25

Ag_2Se	2 min	Yes	Yes	Yes	This work

1. R.-M. Song, Z.-H. Li, P.-J. Wei, X.-L. Zhao, C. Chen and Z.-G. Zhu, *Appl. Sci.*, 2018, **8**.
2. M. Zhang, A. Halder, C. Hou, J. Ulstrup and Q. Chi, *Bioelectrochemistry*, 2016, **109**, 87-94.
3. A. Kothuru, C. H. Rao, S. B. Puneeth, M. Salve, K. Amreen and S. Goel, *IEEE Sens. J.*, 2020, **20**, 7392-7399.
4. C. Zhang, M. Wang, L. Liu, X. Yang and X. Xu, *Electrochem. Commun.*, 2013, **33**, 131-134.
5. S. Nabi, F. A. Sofi, N. Rashid, P. P. Ingole and M. A. Bhat, *New J. Chem.*, 2022, **46**, 1588-1600.
6. F. Salman, A. Zengin and H. Çelik Kazici, *Ionics*, 2020, **26**, 5221-5232.
7. J. Tian, Q. Liu, A. M. Asiri, A. H. Qusti, A. O. Al-Youbi and X. Sun, *Nanoscale*, 2013, **5**, 11604-11609.
8. Y.-C. Yang and W.-L. Tseng, *Anal. Chem.*, 2016, **88**, 5355-5362.
9. Y.-F. Wei, X. Wang, W.-J. Shi, R. Chen, L. Zheng, Z.-Z. Wang, K. Chen and L. Gao, *Eur. J. Med. Chem.*, 2021, **226**, 113828.
10. R.-M. Song, Z.-H. Li, P.-J. Wei, X.-L. Zhao, C. Chen and Z.-G. Zhu, 2018, **8**, 848.
11. J. E. Giaretta, F. Oveissi, F. Dehghani and S. Naficy, *Adv. Mater. Technol.*, 2021, **6**, 2001148.
12. K. V. Ragavan, S. R. Ahmed, X. Weng and S. Neethirajan, *Sens. Actuators B Chem.*, 2018, **272**, 8-13.
13. A. Dutta and U. Maitra, *ACS Sensors*, 2022, **7**, 513-522.
14. W. Fan, Z. Xie and Y. Cui, *Electroanalysis*, 2017, **29**, 1805-1809.
15. S. Pesaran, E. Rafatmah and B. Hemmateenejad, *Biosensors*, 2021, **11**.
16. N. S. K. Gowthaman, P. Arul, J.-J. Shim and S. A. John, *Applied Surface Science*, 2019, **495**, 143550.
17. J. Huang, X. Fang, X. Liu, S. Lu, S. Li, Z. Yang and X. Feng, *Journal of The Electrochemical Society*, 2019, **166**, B814.
18. L. Huang, J. Chen, Z. Yu and D. Tang, *Anal. Chem.*, 2020, **92**, 2809-2814.
19. H. Shang, M. Ding, X. Zhang, A. Zhang, J. Du and R. Zhang, *Chem. Eng. J.*, 2024, **499**, 156392.
20. G. G. Nestorova, B. S. Adapa, V. L. Kopparthy and E. J. Guilbeau, *Sens. Actuators B Chem.*, 2016, **225**, 174-180.
21. Z. Sun, Y. Tong, J. Li, Y. Wang, F. Gao, H. Li, C. Wang, L. Du and Y. Jiang, *Sens. Actuators B Chem.*, 2022, **368**, 132244.
22. Y. Yuan, T. Hu, X. Zhong, M. Zhu, Y. Chai and R. Yuan, *ACS Appl. Mater. Interfaces.*, 2020, **12**, 22624-22629.
23. M. Sattar, Y. J. Lee, H. Kim, M. Adams, M. Guess, J. Kim, I. Soltis, T. Kang, H. Kim, J. Lee, H. Kim, S. Yee and W.-H. Yeo, *ACS Appl. Mater. Interfaces.*, 2024, **16**, 37401-37417.
24. S. Lee, J. Hyun Lee, M. Kim, J. Kim, M.-J. Song, H.-I. Jung and W. Lee, *Applied Physics Letters*, 2013, **103**.
25. B. Hossain, A. K. Paul, M. A. Islam, M. M. Rahman, A. K. Sarkar and L. F. Abdulrazak, *Optik*, 2022, **252**, 168506.